



I S A V

Journal of Theoretical and Applied  
Vibration and Acoustics

journal homepage: <http://tava.isav.ir>



## The effect of shaft-coupling penetration ratio on torsional vibration analysis

Mostafa Irannejadparizi <sup>a,b\*</sup>, Hamed Navabi <sup>b</sup>,  
Pouya Asgharifard Sharabiani <sup>b</sup>, Akbar Naderpour <sup>b</sup>, Saeed Hekmat <sup>b</sup>

<sup>a</sup> Assistant Professor, College of Engineering, University of Tehran, Tehran, Iran.

<sup>b</sup> Rotor-dynamics Researcher, Oil Turbo-Compressor Equipment (OTCE), Tehran, Iran.

Research Article

### ARTICLE INFO

#### Article history:

Received 13 July 2025

Received in revised form 19  
October 2025

Accepted 29 November 2025

Available online 1 June 2026

#### Keywords:

Torsional vibration

Flexible coupling

Torsional Natural Frequencies  
(TNFs)

Shaft Penetration Factor

Finite Element Modeling  
(FEM)

Centrifugal compressor train

### ABSTRACT

When designing typical rotating equipment, torsional natural frequencies (TNFs) must be studied to identify possible resonances. Accurate computation of TNFs and torsional modes requires precise modeling of the shaft-coupling connection. The shaft penetration factor (SPF), representing the shaft's penetration into the coupling hub, significantly affects torsional stiffness calculations. This paper develops a comprehensive torsional vibration software (TVS) for the analysis of a centrifugal compressor train. The torsional analysis of an electrocompressor train, based on API 617 criteria, examines the SPF's effect on torsional output. Five modeling approaches for shaft penetration are considered: SPF values of 0,  $\frac{1}{3}$ ,  $\frac{1}{2}$ , 1, and an end-to-end shaft-coupling connection. The effects of these approaches on the torsional behavior of a real centrifugal compressor train designed by OTCE are investigated. Results show that different modeling approaches change the 2nd and 4th flexible TNFs by about 21% and 13%, respectively, and lead to noticeable differences in mode shapes. The Campbell diagram reveals that intersections of the 2X excitation line with the 2nd and 4th TNFs fall near or within the API separation margin, shifting closer or farther from the critical speed range depending on the modeling approach. Therefore, precise modeling of flexible coupling stiffness is crucial for accurately predicting compressor train torsional natural frequencies, as minor uncertainties in the shaft-coupling connection can lead to significant differences in torsional behavior.

© 2025 Iranian Society of Acoustics and Vibration, All rights reserved.

\* Corresponding author.

E-mail address: [irannejad@ut.ac.ir](mailto:irannejad@ut.ac.ir) (M.Irannejad)

<https://doi.org/10.22064/tava.2025.2065737.1269>

## Nomenclature

I	Moment of Inertia	HS	High Speed
k	Torsional Stiffness	LS	Low Speed
n	Number of Elements	SPF	Shaft Penetration Factor
T	Torque	TNF	Torsional Natural Frequency
$\theta$	Torsional Rotation, Angular Displacement	TVS	Torsional Vibration Software

## 1. Introduction

A centrifugal electrocompressor train typically consists of an electrical motor as the driver, a gear unit as the speed increaser, and a high-speed compressor as the main equipment. The gear unit is connected to the motor and the compressor by two flexible couplings (as shown in 1). A train TNF analysis is necessary for a new compressor train design to identify the locations of the torsional natural frequencies relative to the excitation in the system. Torsional natural frequencies play a key role in identifying potential resonances and designing effective vibration control strategies to prevent system failures. When the train is accurately modeled, undamped torsional natural frequency analysis usually predicts actual train natural frequencies with a small margin of error because most equipment trains have low levels of system torsional damping [1].

Wang et al. [1] studied the effect of variations in mass-elastic data and presented a comparison of measured and predicted TNFs across various cases. Francis et al. [2] compared experimental, theoretical, and computational methods of characterizing torsional stiffness of metallic disk couplings. Zhao et al. [3] studied the factors influencing the torsional stiffness of disc coupling to improve the design and control of rotor torsional vibration. They used finite element modeling to estimate friction and contact behavior in a disc coupling. Song et al. [4] studied the effective diameter of the shrink-fitted shaft-coupling connection. They discussed and compared two modeling methods for the shrink-fit connection: Lamé's equations and the FEA method. An experimental study by Meeus et al. [5] showed that the coupling hub-to-shaft connection significantly influences the system's first torsional mode. By increasing the shaft penetration factor and thus decreasing the hub-to-shaft interference, an eigenfrequency drop and an increase in damping were observed. Venkataraman et al. [6] described a methodology to ensure torsional integrity in standardized Electric-motor-driven gas compressor packages. Mishra et al. [7] analysed torsional vibrations in an open-loop VFD-induction-motor-driven compressor train and proposed methods to reduce them. Ma et al. [8] proposed a torsional vibration simulation model of the loader with variable damping and stiffness. Chen et al. [9] conducted an optimization study of the shaft system structure. They showed that the optimized shaft system increased the 1st-order natural frequency and reduced the peak velocity of the coupling in the vertical direction, thereby improving the service life and operating reliability of the system. Kinnunen et al. [10] introduced a technique for altering torsional natural frequencies via a coupling design that enables continuously adjustable torsional stiffness. The proposed coupling design was tested through torsional analysis and experimental measurements. Kapustin and Degtyareva [11] presented the main stages of torsional vibration calculation for a multi-row reciprocating compressor, including natural and forced vibration analyses. Li et al. [12] explored the sensitivity of the eigen values of the coupling torsional stiffness to the structure-excess, based on the Sobol' method.

Requirements of a torsional system design are normally based on the API Standards [13, 14]. These standards require TNFs to have at least 10% separation margin (SM) from any excitation frequency [1, 13, 14]. To accurately compute the torsional natural frequencies and modes, the torsional characteristics of the different elements of the compressor train must be precisely modeled. One of the complex elements is the shrink-fit connection of the shaft to the coupling hub in flexible elements and dry couplings. Several factors influence the torsional stiffness of a hub-to-shaft connection, including the type of fit (clearance, interference, keyed, or non-keyed), the applied torque, the rotational speed, and the position of the hub flange [14, 15]. The penetration effect of the shaft in the coupling hub, denoted by the shaft penetration factor (SPF), must be considered in the torsional stiffness calculation. Different methods are used to model the torsional characteristics of the hub/shaft connection. There are numerous published criteria and assumptions for modeling the stiffness of flexible couplings. Modeling the stiffness of flexible couplings is essential for accurately simulating the interaction between shafts and components [5].

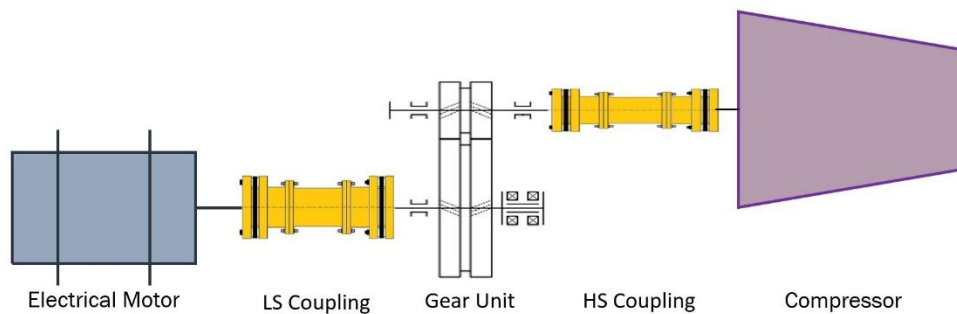


**Fig. 1.** A schematic view of a centrifugal compressor train. The low-speed (LS) coupling connects the driver to the gear unit, and the high-speed (HS) coupling connects the gear unit to the compressor.

In this paper, a comprehensive software is developed for the torsional vibration analysis of a compressor train by the Rotor Dynamics Department of Oil Turbo Compressor Equipment (OTCE) company. The mathematical theory and the reliability of the developed software are validated based on the literature on the physical modeling of the torsional behavior of rotary equipment [16-19]. This in-house software is called TVS (Torsional Vibration Software), hereafter. To study the effects of SPF value on the equipment torsional behavior, a torsional analysis of an electrocompressor train is performed in TVS using five different modeling theories for the shaft-to-coupling hub connection. The five common and widely used modeling approaches chosen in this study span the practical range of penetration used in various industrial modeling applications. The five approaches are as follows:

- Modeling Approach A: “Zero penetration of shaft to coupling hub (SPF = 0).”
- Modeling Approach B: “One-third penetration of shaft to coupling hub (SPF =  $\frac{1}{3}$ ).”
- Modeling Approach C: “Half penetration of shaft to coupling hub (SPF =  $\frac{1}{2}$ ).”
- Modeling Approach D: “Full penetration of shaft to coupling hub (SPF = 1).”
- Modeling Approach E: “End-to-end connection of shaft to coupling hub.”

The effects of these modeling theories on the torsional behavior of the compressor train, i.e., undamped torsional natural frequencies and the corresponding mode shapes, are investigated.

## 2. Materials and methods

This section presents the procedure for developing the torsional finite element model of the compressor train. In addition, the five hub/shaft connection scenarios are schematically presented.

### 2.1. Theory of torsional vibration FEM

This section outlines the essential finite-element stiffness and inertia matrices used in torsional vibration analysis of rotating equipment, including the determination of natural frequencies, mode shapes, etc. Inertia matrices are derived using linear shape functions, and detailed derivations of the equivalent stiffness matrices are provided [17]. Since the gyroscopic coupling between bending and torsional vibrations is primarily nonlinear, this study analyzes torsional vibrations independently of bending behavior, assuming linear system behavior [20-22].

#### 2.1.1. Inertia matrices

Figure 2 illustrates a rotor system consisting of  $n$  uniform elements and  $n+1$  nodes, where each element has a distinct polar moment of inertia, denoted as  $I_1, I_2, \dots, I_n$ .

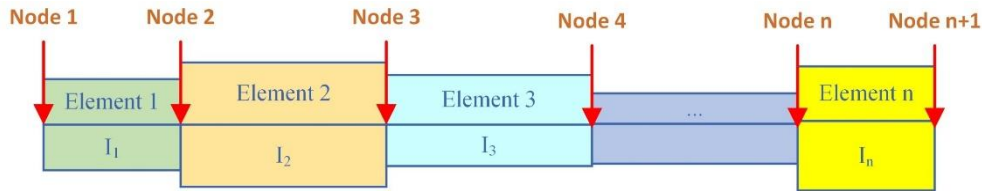


Fig. 2. Rotating equipment finite element model [17].

For each element, half of its total inertia is assigned to each node, resulting in the following global inertia matrix. Formulating an energy-distributed inertia matrix for an element is presented by Walker [17], given as:

$$[I] = \begin{bmatrix} \frac{I_1}{2} & 0 & 0 & \dots & 0 & 0 \\ 0 & \frac{I_1 + I_2}{2} & 0 & \dots & \dots & 0 \\ 0 & 0 & \dots & \dots & \dots & \dots \\ \dots & \dots & \dots & \dots & \dots & \dots \\ \dots & \dots & \dots & \dots & \dots & 0 \\ 0 & \dots & \dots & \dots & \frac{I_{n-1} + I_n}{2} & 0 \\ 0 & 0 & \dots & \dots & 0 & \frac{I_n}{2} \end{bmatrix}_{(n+1) \times (n+1)} \quad (1)$$

The polar moment of inertia of the elements can be defined in terms of their geometric and material properties.

### 2.1.2. Stiffness matrices

For torsional analysis, a torsional spring model is typically sufficient. This section presents the element and global stiffness matrices for systems in which elements have nodes only at their ends. Figure 3 shows the free-body diagram of the element with the stiffness of  $k$ .

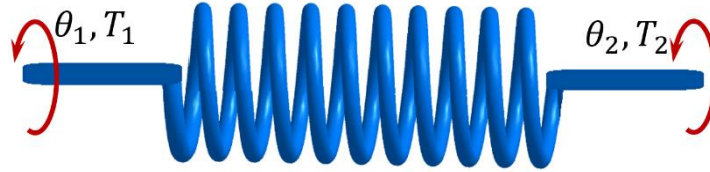


**Fig. 3.** Torsional spring model as an element stiffness [17].

By solving the equilibrium equations, one can express the torques  $T_1$  and  $T_2$  as functions of the nodal displacements,  $\theta_1$  and  $\theta_2$ , as follows.

$$\begin{bmatrix} T_1 \\ T_2 \end{bmatrix} = \begin{bmatrix} k & -k \\ -k & k \end{bmatrix} \begin{bmatrix} \theta_1 \\ \theta_2 \end{bmatrix} \quad (2)$$

The global stiffness matrix for the system depicted in Figure 2 is obtained by assembling the element stiffness matrices.

$$[K] = \begin{bmatrix} k_1 & -k_1 & 0 & \cdot & \cdot & 0 & 0 \\ -k_1 & k_1 + k_2 & -k_2 & \cdot & \cdot & \cdot & 0 \\ 0 & -k_2 & k_2 + k_3 & & & & \cdot \\ \cdot & \cdot & & \cdot & & & \cdot \\ \cdot & \cdot & & & \cdot & & 0 \\ 0 & \cdot & & & & k_{n-1} + k_n & -k_n \\ 0 & 0 & \cdot & \cdot & 0 & -k_n & k_n \end{bmatrix}_{(n+1) \times (n+1)} \quad (3)$$

The element stiffness,  $k$ , can be determined from the material and geometric properties, assuming uniform cross-sectional dimensions and material properties along the element's length.

### 2.1.3. Free vibration analysis

After assembling the global inertia and stiffness matrices ( $[M]$  and  $[K]$ ), the following matrix equation is used to solve the eigenvalue problem and achieve torsional natural frequencies and torsional mode shapes.

$$[I] \begin{bmatrix} \ddot{\theta}_1 \\ \vdots \\ \ddot{\theta}_n \end{bmatrix} + [K] \begin{bmatrix} \theta_1 \\ \vdots \\ \theta_n \end{bmatrix} = 0 \quad (4)$$

## 2.2. Shaft-coupling connection

One common concern in conducting train torsional analysis of rotating equipment using the lumped inertia-stiffness model is the modeling of the shaft-end connection to the coupling hub. The connection of the shaft-end to the coupling hub is typically achieved via a shrink-fit connection, a key connection, or a combination of both. Consequently, the shaft-coupling connection is a friction-connection type and cannot be inferred to be a completely rigid connection. This connection directly affects the system's torsional behavior. Therefore, the method of modeling this connection could be of high importance. Different coupling manufacturers provide torsional stiffness in different ways, as shown in Figure 4. These different modeling approaches are described here:

**Figure 4-A:** In this modeling approach, the total connection length of the shaft to the coupling is considered completely rigid. In other words, the torque is transferred through the shaft only for the part of the shaft that is outside of the coupling, and through the total length of the coupling hub. The shaft section, which is inside the coupling, is rigidly connected to the coupling hub and is considered a part of it. This shaft section does not participate in torque transmission and is modeled as pure inertia, with no torsional stiffness. This approach is called the “**0 penetration**” approach (SPF = 0).

**Figure 4-B:** In this modeling approach, the shaft section inside the coupling hub is considered unrestrained for  $\frac{1}{3}$  of the connection length, and fully rigid for the other  $\frac{2}{3}$  of the connection length. This approach is called the “ **$\frac{1}{3}$  penetration**” rule [1], i.e., SFP =  $\frac{1}{3}$ . The SPF of  $\frac{1}{3}$ , illustrated in Figure 4-F, is the percentage of the shaft length within the confines of the coupling hub that is assumed to be free from restraint at the hub-to-shaft interface. Therefore, the shaft length is effectively increased by the amount of the SPF. Conversely, the length of the coupling hub bore is reduced by the same amount. Based on the hub-to-shaft connection, part of the shaft can twist unrestrained in the coupling hub bore, forming a friction interface [5]. To put it simply, the torque transmits through only the shaft for the first  $\frac{1}{3}$  of the connection length, and through only the coupling hub for the other  $\frac{2}{3}$  of the connection length [15]. In this approach,  $\frac{1}{3}$  of the shaft inside the coupling is modeled as a combination of torsional stiffness and polar inertia. In contrast, the remaining  $\frac{2}{3}$  of this shaft section is modeled as pure inertia.

**Figure 4-C:** This modeling approach is quite similar to the  $\frac{1}{3}$  penetration rule, except that in this method, the SPF is considered to be  $\frac{1}{2}$ . In that case, the shaft section inside the coupling hub is considered unrestrained for half of the connection length, and fully rigid for the other half. Therefore, half of the shaft section inside the coupling hub contributes to torque transmission. The other half of the shaft section does not contribute to the torque transmission and is only modeled as pure inertia. This approach is called the “ **$\frac{1}{2}$  penetration**” method (SFP =  $\frac{1}{2}$ ). In this approach,  $\frac{1}{2}$  of the shaft inside the coupling is modeled as a combination of torsional stiffness and polar inertia. In contrast, the remaining  $\frac{1}{2}$  of this shaft section is modeled as pure inertia.

**Figure 4-D:** In this modeling approach, all the shaft section inside the coupling hub is considered to contribute to the torque transmission. Therefore, this shaft section is modeled as a combination of torsional stiffness and polar inertia. Instead, the length of the coupling that contributes to torque transmission is reduced accordingly. This method can be said to be the opposite of the 0-penetration method. This approach is called the “**Full penetration**” method (SPF = 1).

**Figure 4-E:** In this modeling approach, the connection is modeled in a way that both the shaft section and coupling hub fully contribute to the torque transmission. This method may be called the “end-to-end” method, i.e., the torque travels through the full length of the shaft (to the shaft end), and through the full length of the coupling hub (to the coupling hub end). This approach may be considered a combination of 0-penetration and full-penetration methods.

Most coupling manufacturers consider the shaft end as part of the coupling when calculating the coupling torsional stiffness. This means that coupling manufacturers often calculate coupling stiffness by assuming a fraction of the shaft is penetrated by the coupling hub (e.g., as shown in Figures 4B and C). Specifically, the  $\frac{1}{3}$  penetration rule is frequently used by the coupling vendors.

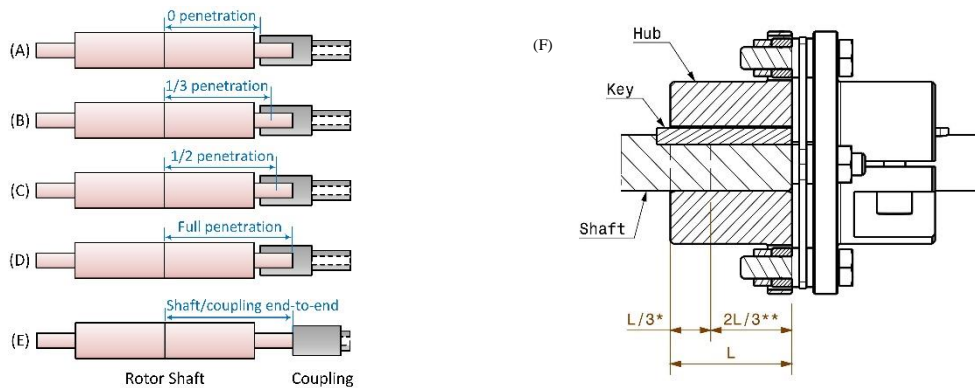


**Fig. 4.** (A) to (D) show different methods for considering the shaft-to-coupling connection torsional stiffness [1]. (F) shows  $SPF = \frac{1}{3}$ , i.e., shaft twists unrestrained for  $\frac{1}{3}L$  and is rigidly connected to the hub for  $\frac{2}{3}L$  [5].

Generally, any other fraction of the shaft section can be considered to be penetrated in the coupling hub when modeling the shaft-coupling connection ( $0 < SPF < 1$ ). Nonetheless, the cases mentioned in Figure 4 are the most common methods. In this paper, the torsional behavior of a compressor train is studied using all five modeling approaches mentioned above, and the results are investigated.

### 2.3. Electrocompressor train

The electrocompressor train, including the motor/gear/compressor, is shown in Figure 1. Different elements of this train are introduced hereafter.

#### 2.3.1. Electrical motor

The driver of the compressor train is an 8.1 MW induction motor. The torsional stiffness and polar moment of inertia of the rotor of this motor are presented in Table 1. The driver's rated speed is presented in Table 1. This data is directly used in modeling the compressor train.

#### 2.3.2. Gear unit

A speed-increasing gear unit is used between the driver and the compressor to increase the compressor speed to the amount specified in Table 1. The cross-sectional drawing of the gear shafts is provided in Figure 5. The torsional characteristics of the gear shafts are provided in Table 1.

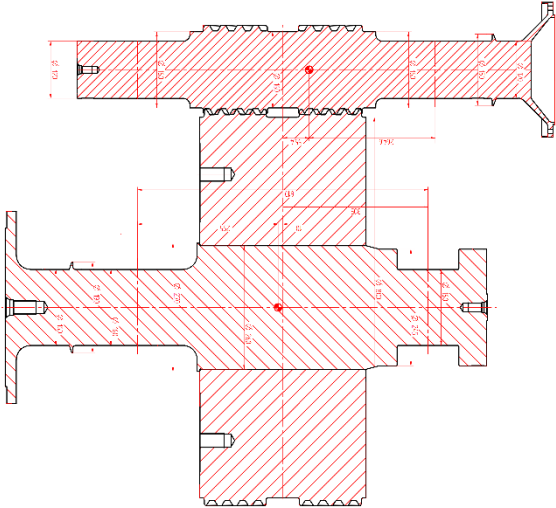


Fig. 5. The cross-sectional drawing of the gear shafts, considered in this paper.

2.3.3. Compressor rotor

The 3D and side views of the compressor rotor, considered in this paper, are shown in Figures 6 and 7, respectively. The compressor is an 8.1 MW unit that compresses the gas in 3 stages. It is designed and manufactured by OTCE. The total polar moment of inertia of the compressor rotor is provided in Table 1.

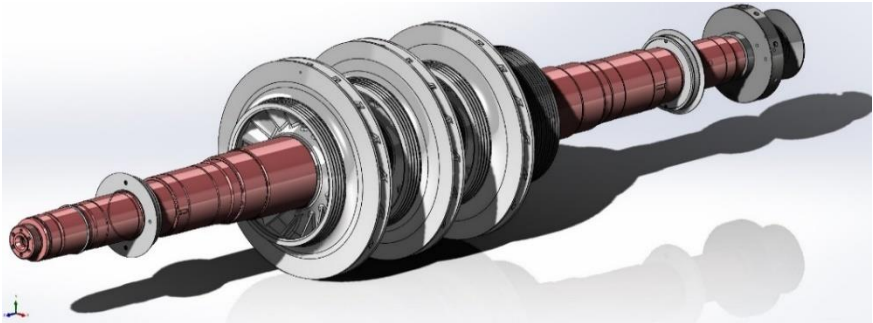


Fig. 6. The 3D view of the compressor rotor, considered in this paper.

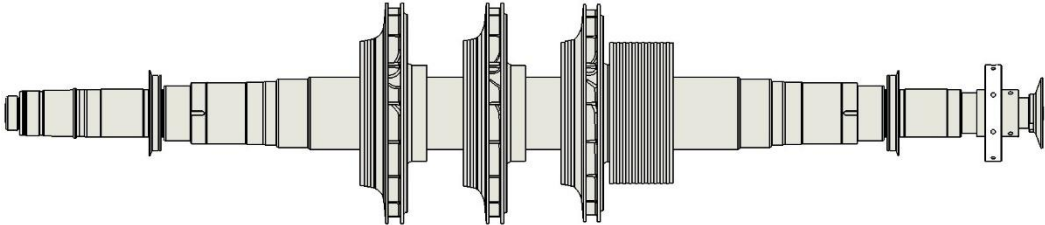
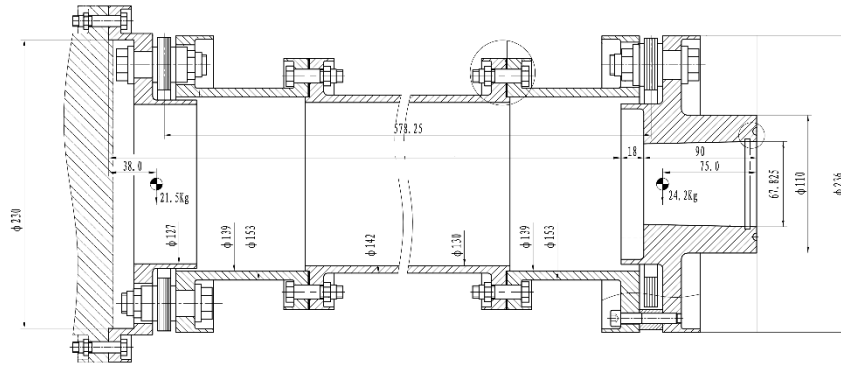


Fig. 7. The side view of the compressor rotor, considered in this paper.

2.3.4. Couplings

The driver is connected to the gearbox via Low-Speed (LS) coupling, and the gearbox is connected to the compressor via High-Speed (HS) coupling. The cross-sectional drawing of the HS coupling is shown in Figure 8. The polar mass moment of inertia of the couplings is provided by the

coupling's vendor, as listed in Table 1. Additionally, the vendor presented the couplings' torsional stiffness, assuming the shaft for the first  $\frac{1}{3}$  penetration. These torsional stiffness values are listed in Table 1. Moreover, based on the geometrical and material properties of the couplings, the torsional stiffness of the HS coupling is calculated for various penetration conditions (i.e., 0 penetration,  $\frac{1}{2}$  penetration, full penetration, and end-to-end) in this paper. The procedure described in AGMA 9004 (1999) is used to calculate the coupling's torsional stiffness for each case. According to AGMA 9004 (1999) [15], the coupling stiffness is obtained by calculating the stiffness of each component along the torque path and summing them as if they were springs in series. The results of the calculations are presented in Table 2.



**Fig. 8.** The cross-sectional drawing of the HS coupling.

### 2.3.5. Assembled motor / gear / compressor train

The compressor train torsional model is developed as shown in Figure 9. The train consists of two branches: the LS and HS branches. The LS branch includes the driver (E-motor), LS coupling, gearbox, LS shaft, and the bull gear, as shown in Figure 9. The HS branch includes the gearbox, HS shaft, HS coupling, and the compressor elements. Different lumped masses along the rotor (e.g., compressor impellers) are modeled as lumped inertias without stiffness (note the solid circles in Figure 9).

Figure 9 shows the developed model when the  $SPF = \frac{1}{3}$  is applied to model the connection between the compressor shaft and the HS coupling. Five different train torsional models are developed using five introduced modeling approaches for the connection of the compressor shaft and the HS coupling. The only difference between the five models is the connection of the HS coupling to the compressor shaft. Figure 10 shows the difference between these five models. Other parts of the models, including HS shaft-to-HS coupling connections and LS coupling connections, are identical.

The rated speed and operating speed range for each branch are presented in Table 3. The compressor is modeled in TVS based on this data.

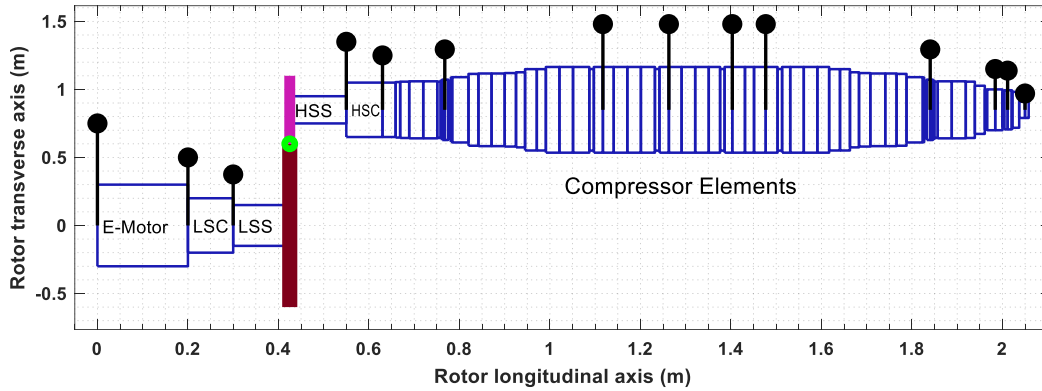


Fig. 9. The developed compressor train torsional model in TVS.

Modeling Approach	The connection of compressor shaft to HSC
A: SPF = 0	
B: SPF = 1/3	
C: SPF = 1/2	
D: SPF = 1	
E: end-to-end	

Fig. 10. The difference in the shaft-coupling connection between five modeling approaches.

Table 1. Torsional stiffness and moment of inertia of the different components of the compressor train.

Component	Torsional Stiffness (MNm/rad)	Moment of Inertia (kg.m <sup>2</sup> )
LS coupling	3.210 (Assuming 1/3 penetration rule)	2.41 (Motor side), 1.06 (Gear side)
HS coupling	3.210 (Assuming 1/3 penetration rule)	0.193 (Gear side), 0.174 (Compressor side)
Gear shaft	13.810	120.5
Pinion shaft	4.300	0.4
E-motor	6.447	135.4
Compressor	-	0.609

**Table 2.** HS coupling torsional stiffness for different modeling approaches, calculated based on AGMA 9004 procedure.

Modeling Approach	HS Coupling Torsional Stiffness (MNm/rad)
A: SPF = 0	1.191
B: SPF = 1/3	1.030
C: SPF = 1/2	0.964
D: SPF = 1	0.837
E: end-to-end	0.837

**Table 3.** Compressor train branches rated speed (operating range is 80% to 105% of these speed values).

No. of Branch	Components	Rated Speed (rpm)	Operating speed range
1	E-motor, LS coupling, Gear shaft	2844	80% to 105% of the rated speed
2	Pinion shaft, HS coupling, Compressor	13392	80% to 105% of the rated speed

### 3. Results and discussion

As described above, five compressor train models were developed here, with five different approaches for modeling the connection between the HS coupling and the compressor shaft. The results presented in this section show the effects of different modeling approaches on the system torsional natural frequencies, torsional mode shapes, and Campbell diagram.

#### 3.1. Torsional natural frequencies

Eight undamped torsional natural frequencies of the compressor train are presented and compared in a clustered-column diagram, in Figure 11, based on different modeling approaches. The first TNF of all models is zero, corresponding to the rigid torsional mode. The other presented TNFs correspond to flexible modes. As the results show, 1st, 2nd, 4th, and 6th TNFs obtained from different approaches are almost equal. On the other hand, different approaches yielded distinct 3rd, 5th, 7th, and 8th TNFs.

To better understand the similarities and differences, all TNFs of different approaches (related to flexible modes 2nd to 8th) are normalized to the TNF values of the 1/3 penetration approach. In other words, the TNFs corresponding to SPF = 1/3 are considered to be 100%, and the TNFs corresponding to other approaches are compared with these 100% values (Figure 12). As the results show, using different modeling approaches has changed the 3rd and 5th TNFs by about 21% and 13%, respectively. The changes in the 7th and 8th TNFs are about 5% and 3%, respectively. According to API 617 [13], the intersection of the primary modes with the 1X mechanical excitation must be at least 10% higher or 10% lower than the designated operating

speed range. Hence, we focus on the 3rd and 5th TNFs, as the variations in these TNFs across different approaches exceed 10% and may conflict with the API requirement.

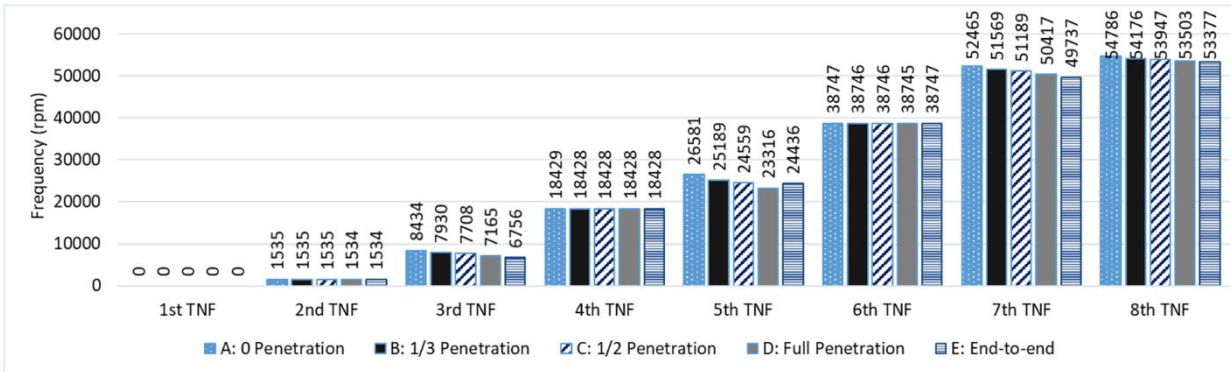


Fig. 11. The compressor TNFs, based on five different modeling approaches.

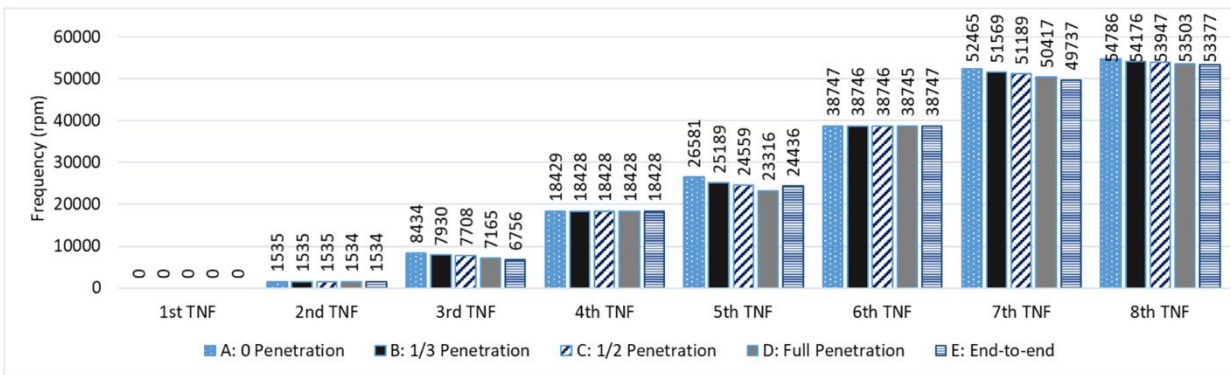


Fig. 12. The compressor TNFs, normalized with respect to the TNF values of the 1/3 penetration approach.

As the results show, in the case that a penetration ratio is considered for the shaft into the coupling, i.e., modeling approaches A to D, as the penetration ratio increases, overall coupling stiffness and the corresponding natural frequency decrease (see Table.2, Figure.11 and Figure.12). It can be inferred that as the penetration ratio increases, the effective length of the coupling hub shortens, the amount of shaft section that is considered as a part of the coupling increases; therefore, overall coupling stiffness decreases.

### 3.2. Torsional mode shapes

In this section, the flexible mode shapes for different TNFs are investigated to better understand the source of differences between the modeling approaches. The eight torsional mode shapes corresponding to the TNFs in Figure 11 are presented in Figures 13-20. The torsional mode shapes are shown in straight and/or broken lines along the rotor's longitudinal axis for different approaches (see the figure legends). For better understanding, the compressor train is also shown in the figures. For brevity, all mode shapes are shown on one rotor model. This does not matter, since the focus of this section is on the mode shapes.

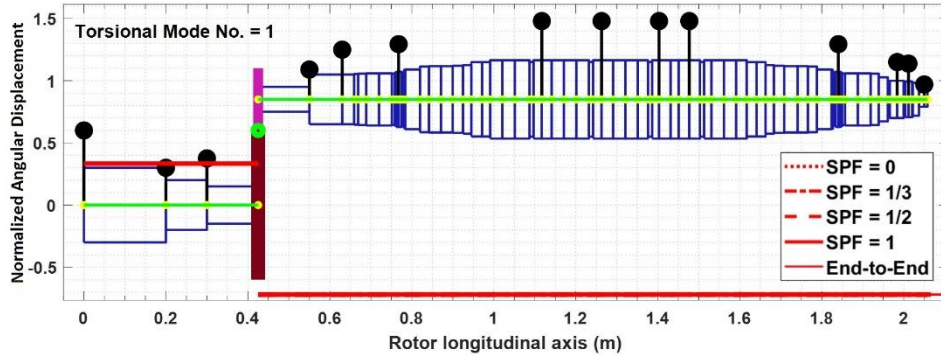


Fig. 13. First torsional mode shape (rigid mode); corresponding to the 1st TNF of Figure 11.

Figure 13 shows the first torsional mode, called the rigid mode. The change of direction and value of the mode shape at the gear node shows the gear ratio. All modeling approaches lead to a similar rigid mode, as they have similar 1st TNS, as well.

The mode shape corresponding to the 2nd TNF Figure 11, namely the first flexible mode shape, is shown in Figure 14. As shown in the figure, in this mode shape, the LS branch of the train (motor, LS coupling, and LS shaft) behaves flexibly. Still, the HS branch (HS coupling, HS shaft, and the compressor) almost behaves as a rigid body (see the straight line of the HS branch in Figure 14). The difference in the modeling approaches was in how the HS coupling was connected to the compressor shaft. In this mode shape, this connection behaves as a rigid body; therefore, we see no difference between the approaches. The corresponding TNF was also the same for all approaches (see 2nd TNF in Figure 11).

The above observation, i.e., the rigid behavior of the HS branch leading to similar results across all modeling approaches, is also observed in the fourth and sixth mode shapes (see Figure 16 and 18). This may be inferred as the main reason for the similarity of the 2nd, 4th, and 6th TNF values.

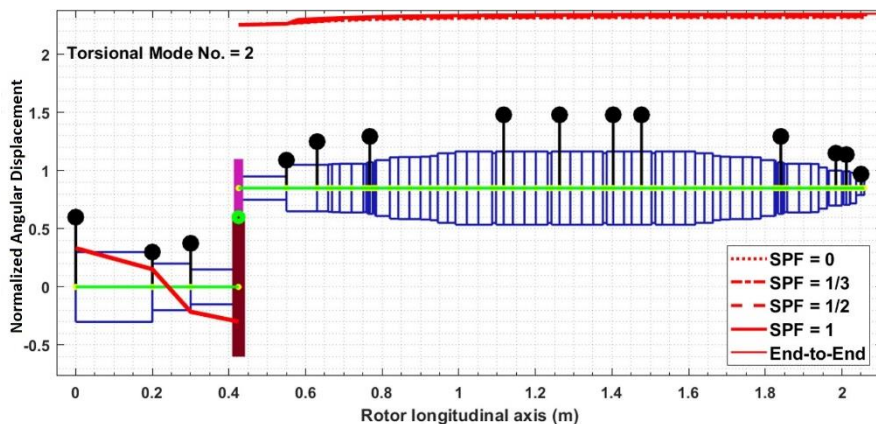


Fig. 14. Second torsional mode shape (first flexible mode); corresponding to the 2nd TNF of Figure 11.

The mode shape corresponding to the 3rd TNF of Figure 11, namely the second flexible mode shape, is shown in Figure 15. As shown in this figure, the LS branch behaves almost rigidly, and the HS branch behaves completely flexible, in this mode. Therefore, this mode shape (like the corresponding TNF) clearly shows the difference between the modeling approaches. The mode

shapes of different approaches differ from each other at the location of the connection of the HS coupling to the compressor rotor. The more the shaft is considered to be penetrated to the coupling (SPF = 0 to SPF = 1), the less the total coupling stiffness (Table 2), the less the TNF (Figure 11), and the more the deflection of the mode shape (Figure 15).

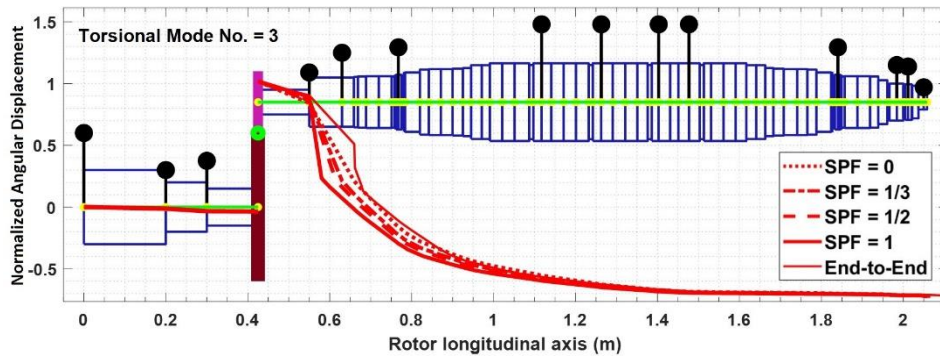


Fig. 15. Third torsional mode shape (second flexible mode); corresponding to the 3rd TNF of Figure 11.

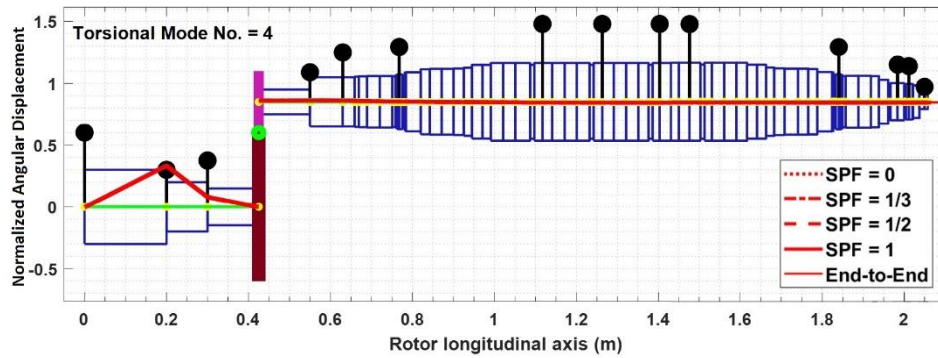


Fig. 16. Fourth torsional mode shape (third flexible mode); corresponding to the 4th TNF of Figure 11.

The mode shape corresponding to the 5<sup>th</sup> TNF, namely the fourth flexible mode shape, is shown in Figure 17. As shown in the figure, the HS branch behavior in this mode is quite flexible. All HS items, namely the HS shaft, HS coupling, and the compressor rotor, play the main vibrational role of this torsional mode. Therefore, it is expected that different modeling approaches will affect the TNF associated with this mode shape. As the penetration ratio increases from 0 to 1, deflection increases in the region of HS coupling to the shaft connection.

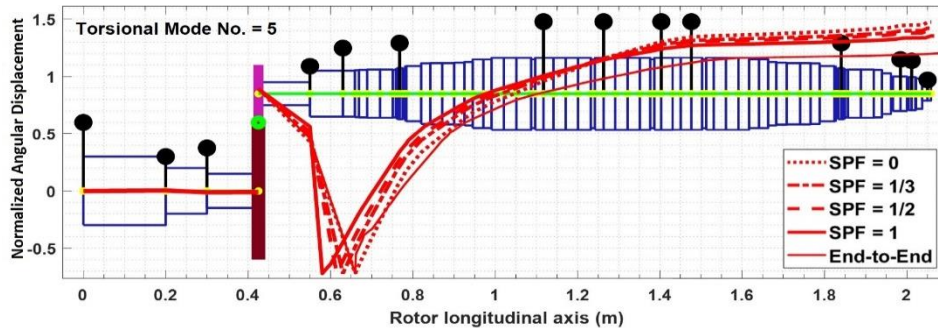


Fig. 17. Fifth torsional mode shape (fourth flexible mode); corresponding to the 5th NF of Figure 11.

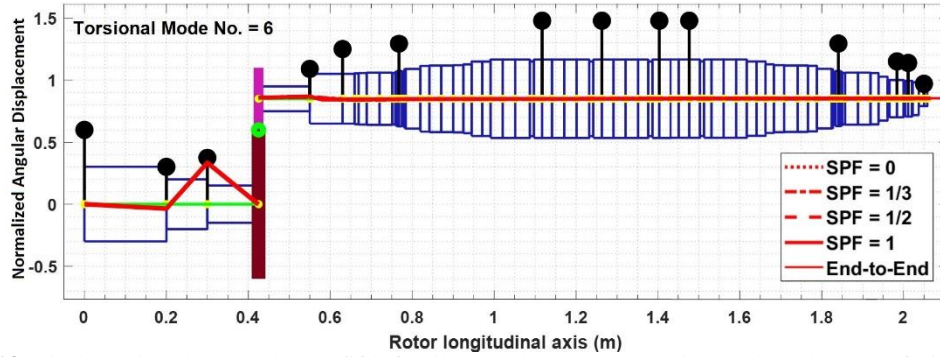


Fig. 18. Sixth torsional mode shape (fifth flexible mode); corresponding to the 6th TNF of Figure 11

Figure 19 and Figure 20 show the mode shapes corresponding to the 7<sup>th</sup> and 8<sup>th</sup> TNFs, for different modeling approaches. In both mode shapes, the flexibility of the HS coupling is clearly observed. Therefore, the effects of differences between modeling approaches become more pronounced, and different approaches yield distinct deflections in the mode shapes.

Another point observed from the 7th and 8th mode shapes is that the deflection of the mode shape corresponding to the end-to-end modeling approach is significantly different from those of other approaches. The reason for this observation may be the weakness at the connection node of the HS coupling and the compressor shaft. Although in the end-to-end approach, the stiffness of the total coupling hub length and total shaft length is considered in the calculation, the connection node is somewhat weak due to the weakness of the shaft end elements (see Figure 10). It seems this weakness could lead to large deflections in the mode shape near the connection between the HS coupling and the compressor shaft.

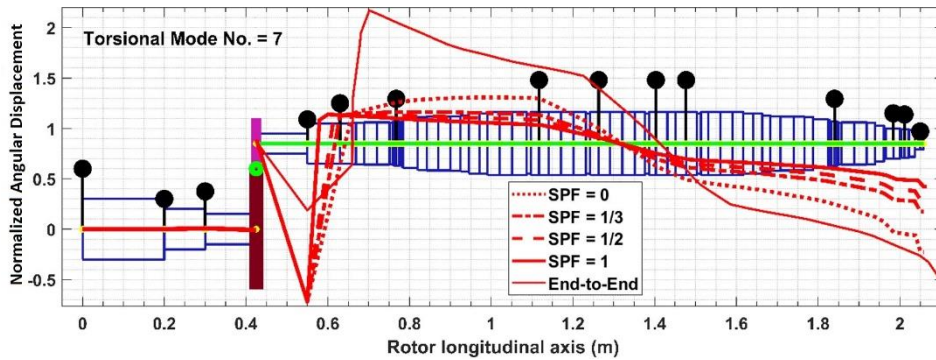


Fig. 19. Seventh torsional mode shape (sixth flexible mode); corresponding to the 7th TNF of Figure 11.

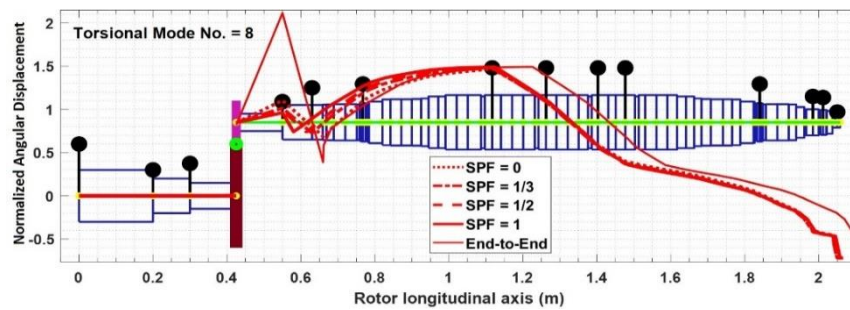


Fig. 20. Eighth torsional mode shape (seventh flexible mode); corresponding to the 8th TNF of Figure 11.

### 3.3 Campbell diagram

In this section, the Campbell diagram is analysed to observe the effects of different modeling approaches more comprehensively. Figure 21 shows the Campbell diagram developed by TVS for the compressor train modeled using approach B ( $SPF = \frac{1}{3}$ ). The horizontal axis shows the speed in rpm. The flexible TNFs (2nd TNF to 8th TNF) are specified on the vertical axis (see the horizontal lines in the plot). Two vertical solid lines show the rated speeds of the LS and HS branches of the compressor train (see 3). Two vertical dashed lines specify the operating speed range of the LS and HS branches, i.e., 80% to 105% of the rated speed. The two diagonal lines are the 1X and 2X compressor operation lines.

The intersection of the diagonal lines with each horizontal line shows a speed that may be a cause for concern. According to API 617, “the intersection of the primary (coupling) modes with the 1X mechanical excitation shall be at least 10 % above or 10 % below the specified operating speed range”. The range of 10 % above and 10 % below the specified operating speed range is shaded in the Campbell diagram (see the shaded areas in Figure 21). A similar Campbell diagram is shown in Figure 22, where the TNF values for all modeling approaches are depicted (see the horizontal lines and the figure legend).

As seen from Figure 21, the intersections of the 1X line with the first and second natural frequencies (the primary critical speeds) do not fall within the shaded area. It can be interpreted that the compressor train meets API torsional requirements. As shown in Figure 22, the intersection of the 1X line with the primary TNFs across all modeling approaches remains well outside the shaded area. Nonetheless, some approaches bring this intersection closer to the API margins.

To investigate the effect of different modeling approaches more deeply, we examine the 2X line and its intersections with the presented natural frequencies. As the results show, when the compressor train is modeled based on approach B,  $SPF = \frac{1}{3}$  (Figure 21), the intersection of the 2X line with the 3rd TNF falls near the border of the shaded/critical area (note the left arrow in Fig.). On the contrary, modeling the compressor using other approaches causes the intersection of the 2X line with the 3rd TNF to get closer to or away from the shaded area (note the left arrow in Figure 22). Modeling approach A ( $SPF = 0$ ) moves the intersection away from the shaded area, whereas approaches C and D move it closer to the shaded area. The E (end-to-end) modeling approach causes the intersection of the 2X line with the 3<sup>rd</sup> TNF to almost touch the shaded area.

Moreover, in the case of  $SPF = \frac{1}{3}$ , the intersection of the 2X line and the 5th TNF falls almost in the midrange of the compressor operating range (see the right arrow in Figure 21). While in cases of  $SPF = \frac{1}{2}$ ,  $SPF = 1$ , and end-to-end, this intersection is moved toward the border of the shaded area. In case of  $SPF = 0$ , this intersection crosses the rated speed of the compressor (note the right arrow in Figure 22).

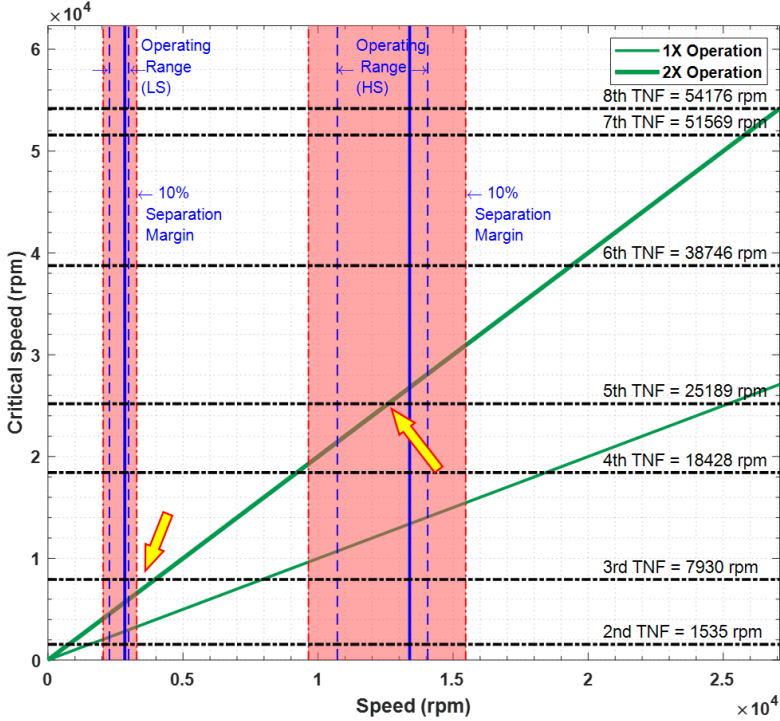


Fig. 21. Campbell diagram for modeling approach B (SPF = 1/3).

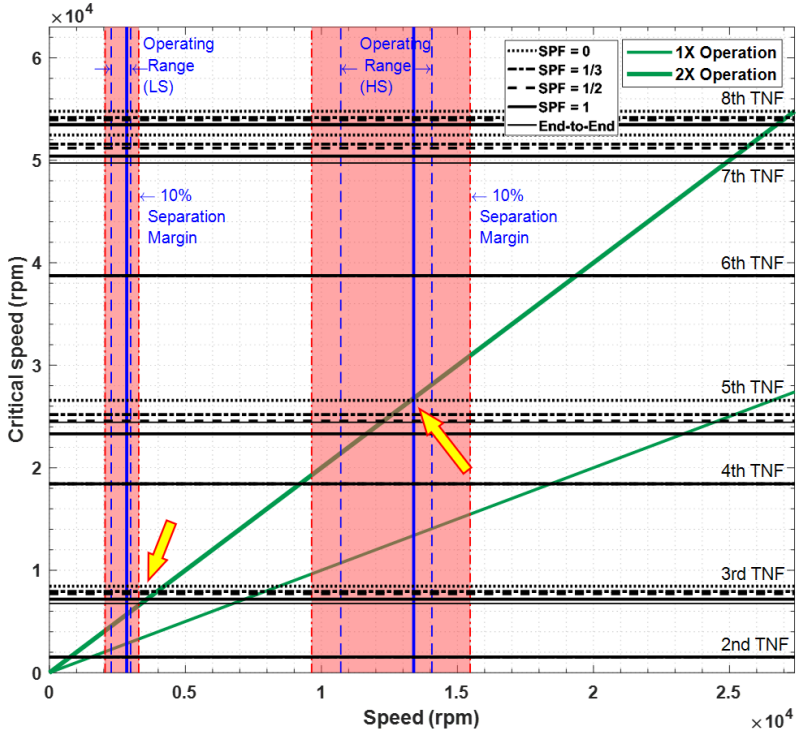


Fig. 22. Campbell diagram considering all modeling approaches A to E.

As the results show, when we use different approaches in modeling the connection of the coupling to the shaft, considerable effects on some of the torsional natural frequencies of the model are observed. Variation of the TNFs may cause the model to conflict with the API margins. If we consider different modeling approaches for other coupling connections (e.g., LS coupling connections), more TNFs are affected and torsional analysis issue gets more complicated.

## **4. Conclusion**

A new compressor train design requires a train torsional natural frequency (TNF) analysis. In this study, a comprehensive torsional vibration software is developed to provide the necessary tools and understanding for TNF analysis of rotor trains. The results, which show reasonable behavioral changes compared with changes in stiffness due to SPF, will then certify the usefulness of the developed tools. The torsional analysis of an electrocompressor train is then carried out to investigate the effects of the shaft penetration factor (SPF) on the torsional behavior of a real compressor train, in accordance with API-617 criteria. Five different modeling approaches for the shaft-to-coupling hub connection are considered to model the torsional behavior of the compressor train. Modeling approach A considers “zero penetration of the shaft in the coupling hub (SPF = 0)”. Approach B considers “ $\frac{1}{3}$  penetration of the shaft in the coupling hub (SPF =  $\frac{1}{3}$ )”. Approaches C and D consider SPF =  $\frac{1}{2}$  and SPF = 1, respectively. Modeling approach E considers “end-to-end shaft-coupling connection”. More approaches are available in the literature for this friction connection between the shaft and coupling hub. Every modeling approach can have its own philosophy and justification. To observe the differences among five models, undamped TNFs, corresponding mode shapes, and the Campbell diagram of the system are investigated.

As the results show, changing the modeling approach will change some TNFs. In the compressor train of this study, the 3rd, 5th, 7th, and 8th TNFs show variations of about 21%, 13%, 5%, and 3%, respectively, due to changes in the modeling approach. The corresponding mode shapes also show noticeable differences between different SPF values. These TNFs correspond to the mode shapes, which show flexibility at the coupling-shaft connection. Other TNFs and mode shapes were not affected by changing the shaft-to-coupling connection modeling. In the modeling approaches that consider a penetration ratio for the shaft into the coupling, as the penetration ratio increases, a decrease in the corresponding TNF(s) is observed.

The Campbell diagram shows that when the compressor train is modeled using different approaches, the intersections of the 1X and 2X lines with the TNFs, i.e., the resonance potentials of the system, change. Approach B (SPF =  $\frac{1}{3}$ ) causes the intersection of the 2X line with the 3<sup>rd</sup> TNF fall near the API 617 separation margin. Modeling approach A moves this intersection away from the API margin, while approaches C and D move it closer to the margin. Modeling approach E causes the intersection of the 2X line with the 3<sup>rd</sup> TNF to almost touch the API margin.

In the case of approach A, the intersection of the 2X line and the 5th TNF is almost equal to the compressor rated speed. Although other approaches (B to E) move this intersection farther from the compressor's rated speed, it remains within the API margin.

To sum up, the correct modeling of the shaft-coupling connection is very important for accurately addressing the compressor train's torsional natural frequencies. Minor uncertainties in the modeling approach may lead to noticeable differences in the torsional behavior of the equipment's model. Uncertainties can narrow the allowable operating speed range of the equipment to avoid

exceeding the API margins. If the modeling approach is not accurately selected, then the accuracy of torsional vibration analysis would be low, and the error in estimating TNFs would be significant. This issue may presumably reduce the validity of the analysis. Although some modeling approaches are better known and more widely used, a deeper analysis of the physical characteristics of the shaft-coupling connection is required better to understand the accuracy of model simulations of real behavior.

## Acknowledgement

The authors thank Mr. Seyed Mohammad Hossein Dibajee and Mr. Mahdi Arezoomand, at OTCE design office for their kind understanding, encouragement, and support in completing this project.

## References

- [1] Q. Wang, B.C. Pettinato, T.D. Feese, Torsional natural frequencies: measurement vs. prediction, *42nd Turbomach. Symp*, Texas, USA, Vol.,(2013), September 30 – October 3, 2013.
- [2] A. Francis, I. Avdeev, J. Hamann, S. Ananthasivan, Accurate characterization of torsional stiffness of flexible disk couplings, *Journal of Engineering for Gas Turbines and Power*, Vol. 137, Iss.8,(2015)
- [3] B. Zhao, Y. Zhao, J. Feng, X. Peng, Numerical and experimental investigation of the torsional stiffness of flexible disc couplings, *International Journal of Mechanical Sciences*, Vol. 114,(2016)
- [4] W. Song, Z. Liu, Q. Lu, A study on effective diameter of shrink-fitted shaft-hub connection, in *International Conference on Advanced Mechatronic Systems (ICAMechS)*, 2017: IEEE, pp. 274-279. [Online]. Available: <https://doi.org/10.1109/ICAMechS.2017.8316484>
- [5] H. Meeus, B. Verrelst, D. Moens, P. Guillaume, D. Lefeber, Experimental study of the shaft penetration factor on the torsional dynamic response of a drive train, *Machines*, Vol. 6, Iss.3,(2018)
- [6] B. Venkataraman, R. Kurz, M. Vagani, J. Mistry, G.J. Cole, Torsional vibrations in electric motor driven compressor trains, in *2019 IEEE Petroleum and Chemical Industry Committee Conference (PCIC)*, 2019: IEEE, pp. 277-284. [Online]. Available: <https://doi.org/10.1109/PCIC30934.2019.9074771>
- [7] S. Mishra, A.B. Palazzolo, X. Han, Y. Li, C. Kulhanek, Torsional vibrations in open loop volts hertz variable frequency drive induction motor driven mechanical systems, in *2020 IEEE Texas power and energy conference (TPEC)*, 2020: IEEE, pp. 1-6. [Online]. Available: <https://doi.org/10.1109/TPEC48276.2020.9042586>
- [8] W. Ma, D. Xie, Z. Wang, Z. Ran, C. Liu, S. Wang, Modeling, calculation, and analysis of torsional vibration characteristics of the hydrodynamic transmission system in engineering vehicle, *Proceedings of the Institution of Mechanical Engineers, Part D: Journal of Automobile Engineering*, Vol. 236, Iss.8,(2022)
- [9] Z. Chen, S. Nie, T. Li, T. Lai, Q. Huang, K. Zhang, Torsional vibration response characteristics and structural optimization of shale gas compressor shaft system, *Proceedings of the Institution of Mechanical Engineers, Part E: Journal of Process Mechanical Engineering*, Vol. 236, Iss.3,(2022)
- [10] K. Kinnunen, S. Laine, T. Tiainen, R. Viitala, Method for adjusting torsional natural frequencies of powertrains with novel coupling design, *Machines*, Vol. 10, Iss.3,(2022)
- [11] P. Kapustin, T. Degtyareva, Torsion vibration calculation in reciprocating compressors, in *2022 International conference on Dynamics and Vibroacoustics of Machines (DVM)*, 2022: IEEE DVM, pp. 1-7. [Online]. Available: <https://doi.org/10.1109/DVM55487.2022.9930885>

- [12] T. Li, Z. Huang, Z. Chen, J. Wang, C. Wang, Study on the torsional stiffness and vibration response law of laminated coupling considering the effect of excess, *Mechanical Systems and Signal Processing*, Vol. 222,(2025)
- [13] API Standard 617: Axial and centrifugal compressors and expander-compressors, ninth ed, 2014.
- [14] API Standard 684: Tutorial on the API Standard paragraphs covering rotor dynamics and balancing: An introduction to lateral critical and train torsional analysis and rotor balancing, 2005.
- [15] AGMA 9004-A99. Flexible couplings—Mass elastic properties and other characteristics, A.G.M. Association, 1999.
- [16] E. Nestorides, A handbook on torsional vibration, Cambridge University Press, 1958.
- [17] D.N. Walker, Torsional vibration of turbomachinery, McGraw-Hill, New York, 2004.
- [18] M.L. Adams, Rotating machinery vibration: from analysis to troubleshooting, CRC Press, 2009.
- [19] J.M. Vance, F.Y. Zeidan, B.G. Murphy, Machinery vibration and rotordynamics, John Wiley & Sons, 2010.
- [20] E. Sghaier, A. Bourdon, D. Remond, J.-L. Dion, N. Peyret, Coupled bending torsional vibrations of non-ideal energy source rotors under non-stationary operating conditions, *International Journal of Mechanical Sciences*, Vol. 163,(2019)
- [21] M.A. Corbo, S.B. Melanoski, Practical design against torsional vibration, Vol.,(1996)
- [22] Q. Li, C. Chen, S. Gao, Y. Ren, W. Wang, The coupled bending-torsional dynamic behavior in the rotating machinery: modeling, simulation and experiment validation, *Mechanical Systems and Signal Processing*, Vol. 178,(2022)